Int. J. Electrochem. Sci., 15 **(2020)** 371 – 381, doi: 10.20964/2020.01.17

International Journal of
ELECTROCHEMICAL
SCIENCE
www.electrochemsci.org

Green Synthesis of Polypyrrole coated Manganesee(II) Vanadate Nanoflower Composite as Cathode Materials

Hao Zhu[1,2], Lai Ma[1,2], Jian Jiang[1,2], Zemin Xia[1], Xi He[1], Jiao Yang[1], Baodeng Yang[1], Qing Li[1,2,]*

[1] Key Laboratory of Luminescent and Real-
Time Analytical Chemistry (Ministry of Education), School of Materials and Energy, Southwest University, Chongqing 400715, China
[2] Chongqing Key Laboratory for Advanced Materials and Technologies of Clean Energies, Southwest University, Chongqing 400715, China
[*]E-mail: qli@swu.edu.cn

Received: 8 August 2019 / *Accepted:* 8 October 2019 / *Published:* 30 November 2019

Flower-like $Mn(VO_3)_2$ precursors were synthesized by a hydrothermal method. Then they were wrapped by Polypyrrole (PPy) to obtain uniform $Mn(VO_3)_2$ @PPy nanoflower composites, which were consist of nanosheets with a length of 150-300 nm and covered with a layer of PPy. The $Mn(VO_3)_2$ @PPy nanoflower composites had a discharge capacity of 102.6 mAh g^{-1} range of 1.5-4.5 V at a current density of 0.1 A g^{-1} and a specific discharge capacity of 75.3 mAh g^{-1} range of 1.5-4.5 V when the current density was 1 A g^{-1}. After 500 cycles, their coulomb efficiency was close to 100%, exhibiting good cycle performance. These results indicated that the $Mn(VO_3)_2$ @PPy nanoflower composites are promising as a lithium ion cathode material with good recycling performance.

Keywords: $Mn(VO_3)_2$ @PPy; nanoflower; Cathode material

1. INTRODUCTION

With the development of science and technology, electronic products are becoming more and more important [1-4]. At the same time, the energy storage problem brought by new electronic devices is more prominent, which bring about an urgent need to study new energy storage systems [5, 6]. As an important part of energy storage system, lithium ion battery becomes the focus in recent decades [4, 7]. However, traditional cathode materials of lithium ions have some problems, such as lack of safety, high cost or poor cycling stability. Therefore, it is necessary to develop new cathode material of lithium ion.

The coated conductive polymer can effectively increase the activity of the battery cathode material. As a conductive polymer, Polypyrrole (PPy) is widely used because of its good electrical

conductivity and excellent stability. The coating of PPy greatly enhances the performance of the electrode material and gives full play to the original electrochemical performance of the material [8-13].Most importantly, PPy acts as a conductive agent to reduce resistance to ion migration while protecting the structure of the active material.

Vanadium bronze is an important ternary oxide. As a lithium ion battery material, vanadium bronze has the characteristics of high capacity [14], low cost and easy preparation [15-21]. The structure of the electrode material has an important influence on electrochemical performance. In order to achieve good performance, it is still a challenge to explore a vanadium-based bronze having a novel structure for use as an electrode material for lithium ion battery. Compared with the previously fabricated nano powder [22], nanowires [23, 24], or nanobelt of MnV_2O_6 [25], the flower-like structure of $Mn(VO_3)_2$ is worthy of exploration as a new structure.

In this work, $Mn(VO_3)_2$ @PPy nanoflower composites were successfully prepared. Flower-like $Mn(VO_3)_2$ precursors were synthesized by a hydrothermal method. Then, the $Mn(VO_3)_2$ @PPy nanoflower composites were prepared by surface modification, in which the obtained flower-like $Mn(VO_3)_2$ precursors were coated with a layer of PPy on the surface. Furthermore, the optimal preparation time for nanoflower precursors and the effect of anions in the reactants on the product have been explored. Characterizations of the electrochemical properties were performed. It was found that $Mn(VO_3)_2$ @PPy nanoflower composites have good electrochemical performance that they are potentially to be an ideal cathode materials for lithium ion batteries.

2. EXPERIMENTAL DETAILS

2.1. Chemicals

Ammonium metavanadate (NH_4VO_3, M=116.99, 99%), Manganese chloride tetrahydrate ($MnCl_2·4H_2O$, M=197.91, 99.0%), Manganese sulfate monohydrate ($MnSO_4·H_2O$, M =169.02, 99%), Manganese acetate tetrahydrate ($MnC_4H_6O_4·4H_2O$, M=245.09, 99%) Ethylene glycol ($C_2H_6O_2$, M=62.07, ≥99%), Sodium p-toluenesulfonate ($C_7H_7NaO_3S$, M=194.18, 90%), Ammonium persulfate ($(NH_4)_2S_2O_8$, M=28.201, 99%), Pyrrole (C_4H_5N, M=67.09, 99%). The reagents used in the experiments are all analytical reagents and have not been further purified.

2.2. Synthesis of flower-like $Mn(VO_3)_2$ precursors

Flower-like $Mn(VO_3)_2$ precursors were synthesized by a hydrothermal method. Under agitation, $MnCl_2·4H_2O$ (2 mmol) was dissolved in beaker A (5ml, Ethylene glycol: water = 1:1), while NH_4VO_3 (4 mmol) was dissolved in beaker B (30 ml, Ethylene glycol: water = 1:1). Then the solution of A and B were mixed in beaker C. Then the solution in beaker C was transferred into an autoclave. The autoclave was sealed and kept at 120 ℃ for 12 h, and then cooled to room temperature in air. After that, the precipitates were dried at 60 ℃ for 6 h to get the product. The as-prepared products were annealed at 450 ℃ for 4 h to obtain the final $Mn(VO_3)_2$ powders.

2.3. Synthesis of $Mn(VO_3)_2$@PPy Nanoflower Composites

14.5 mg Sodium p-toluenesulfonate and 20 μL pyrrole monomer were dissolved in 35 mL deionized water and stirred for 1 h. 40 mg of flower-like $Mn(VO_3)_2$ precursors were added to the solution and stirred for 0.5 h. Then 15 mL (0.48 mmol L^{-1}) of ammonium persulfate was dispersed into the solution, and continued stirring for 2 h. After that, the above solution was allowed to stand for 6 h. The above experiment was carried out at 0 °C. In the end, the precipitation was washed and dried in a vacuum oven for 12 h to obtain the samples.

2.4. Characterization

The phase structure was investigated by X-ray powder diffraction (XRD) (XD3 system, Beijing Purkinje General Instrument Co., Ltd.) with Cu Kα (λ=0.15406 Å) radiation with the scanning rate of 2° min^{-1}, ranging from 10° to 60° and Fourier transform infrared spectroscopy (FTIR, Nicolet 6700). The morphology was observed by the field emission scanning electron microscopy (FESEM, JSM-6700F), while the energy dispersive X-ray spectroscopy (EDS) was used to describe the chemical element.

2.5. Electrochemical Performance Measurement

$Mn(VO_3)_2$ @PPy nanoflower composites were assembled into a lithium-ion battery as a lithium battery cathode material to study its electrochemical performance. Firstly, $Mn(VO_3)_2$ @PPy nanoflower composites, Poly-(vinylidene fluoride) (PVDF) binder, and Carbon black were mixed in mass ratio of 7:1.5:1.5 and dispersed in N-methyl-2-pyrrolidone (NMP) to form slurries. Then, the above slurry was uniformly applied and prepared on an aluminum with a diameter of 10 mm in advance, and placed in vacuum oven at 80 °C for 12 h. After that, the battery was assembled in an Ar-filled glovebox. Li foil was used as reference and counter electrode, and the solution of 1 M $LiPF_6$ dissolved in a mixture of Diethyl carbonate (DEC) and Ethylenecarbonate (EC) (DEC:EC=1:1) serves as the electrolyte. Electrochemical measurements were conducted by using a CHI 760E Electrochemical Workstation (CH Instruments, China) at room temperature. Cyclic voltammetry (CV), constant current charging, and electrochemical impedance spectroscopy (EIS) were performed. The CV test was performed in the range of 1.5-4.5 V and the scan speed was 0.2 mV s^{-1}. The EIS was performed between 0.01 Hz and 1000 kHz with voltage of 5 mV and the initial voltage was the open circuit voltage.

3. RESULTS AND DISCUSSION

3.1. Characterization of flower-like $Mn(VO_3)_2$ precursors and $Mn(VO_3)_2$ @PPy Nanoflower Composites

The phase and structure of the products were examined by X-ray diffractometer (XRD). Fig. 1a shows the XRD pattern of the precursor which is synthesized at 120 ℃ for 12 h by a hydrothermal

method and calcined at 450°C. All the diffraction peaks can be readily indexed to a pure monoclinic phase of $Mn(VO_3)_2$ (JCPDS Card No. 35-0139). Fig. 1b shows the XRD pattern of the product that coated with PPy. All the diffraction peaks can be indexed to a monoclinic phase of $Mn(VO_3)_2$ (JCPDS Card No. 35-0139). Meanwhile, a platform appears in front of the XRD pattern. According to previous reports, this is caused by PPy [26, 27].

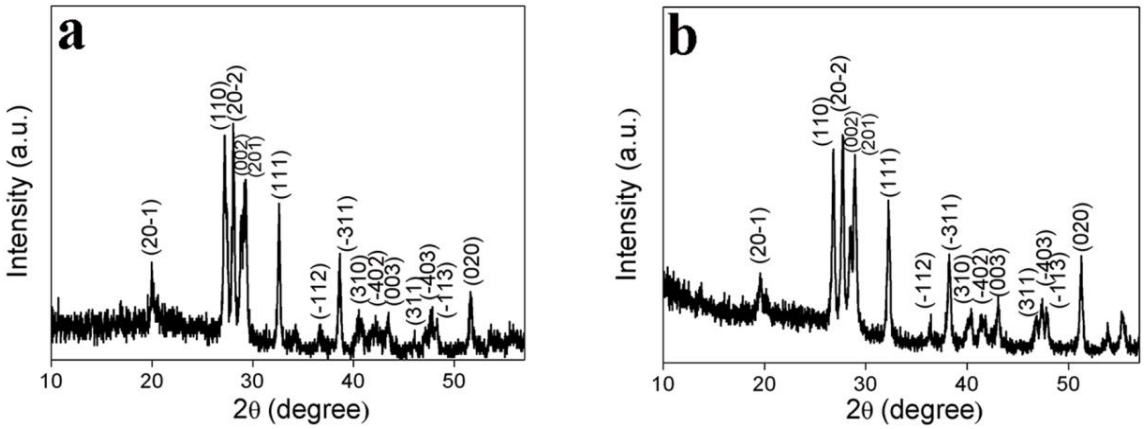

Figure 1. (a) XRD pattern of flower-like $Mn(VO_3)_2$ precursors; (b) XRD pattern of $Mn(VO_3)_2$ @PPy nanoflower composites.

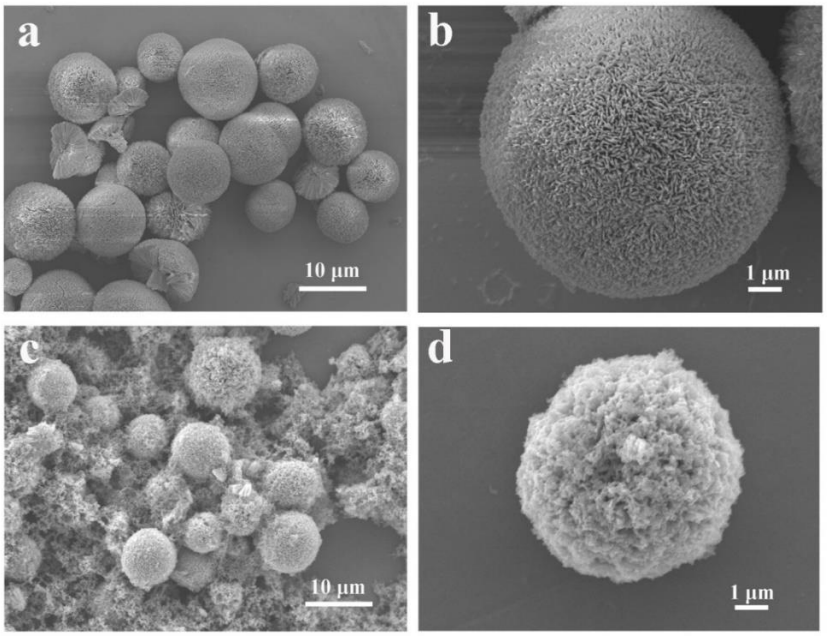

Figure 2. (a) Typical FESEM image of the flower-like $Mn(VO_3)_2$ precursors; (b) High-magnification FESEM image of the flower-like $Mn(VO_3)_2$ precursors; (c) Typical FESEM image of the $Mn(VO_3)_2$ @PPy nanoflower composites (d) High-magnification FESEM image of the $Mn(VO_3)_2$ @PPy nanoflower composites.

Fig. 2a is the typical FESEM image of the flower-like $Mn(VO_3)_2$ precursors after calcination. It can be clearly seen that the shape is nanoflower. These nanoflowers have a diameter of 5-10 μm. Fig. 2b is the higher magnification FESEM image of $Mn(VO_3)_2$ nanoflower precursor. It is observed that the petals of nanoflower are very thin. The thickness of the petals is only a few tens of nanometers and the length is several hundred nanometers. Fig. 2c and Fig. 2d are FESEM images of $Mn(VO_3)_2$ @PPy nanoflower composites. It can be seen that PPy formed a film on flower-like $Mn(VO_3)_2$ precursors, which did not change the morphology of the precursors. Compared to flower-like $Mn(VO_3)_2$ precursors, the $Mn(VO_3)_2$ @PPy nanoflower composites have a layer of small beads on the surface.

Fig. 3 is the FESEM-EDS images of the $Mn(VO_3)_2$ @PPy nanoflower composites. It is found that the patterns mapped by the O, Mn and V elements are all circular, which is consistent with the shape of the nanoflower, indicating that the three elements were evenly distributed in the $Mn(VO_3)_2$ @PPy nanoflower. Meanwhile, it can be observed that the C and S elements also exhibit the same shape as the nanoflower, indicating that the PPy coated uniformly.

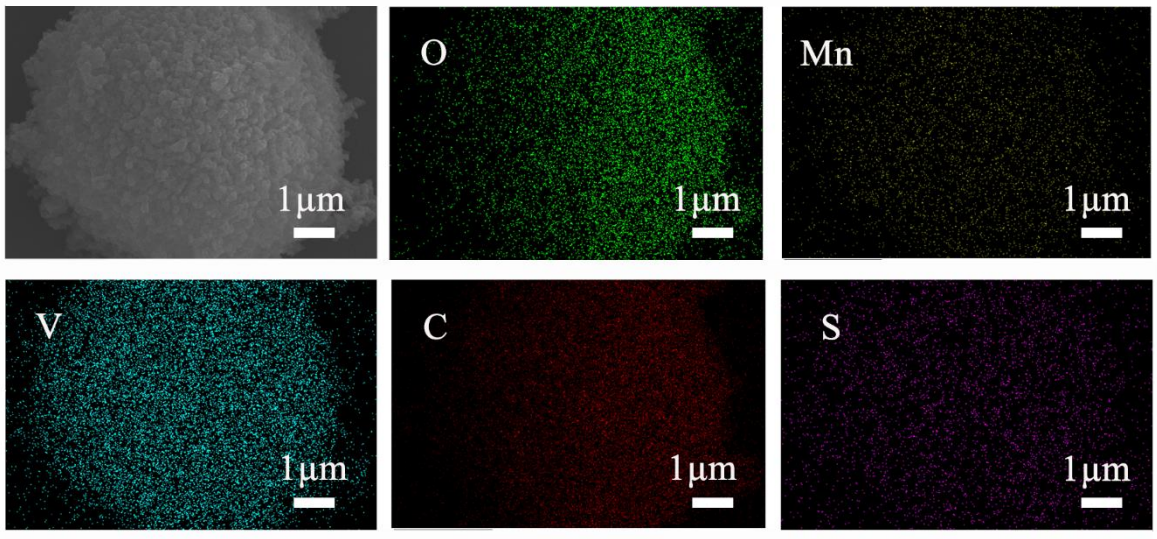

Figure 3. FESEM-EDS images of the $Mn(VO_3)_2$ @PPy nanoflower composites.

FT-IR spectra of the prepared $Mn(VO_3)_2$ @PPy and $Mn(VO_3)_2$ are shown in Fig. 4. Compared to $Mn(VO_3)_2$, the material coated with PPy shows some additional peaks. These peaks can be attributed to the characteristic peaks of PPy : the bands at 1585 cm^{-1} and 1401 cm^{-1} are attributed to the antisymmetric and symmetric pyrrole ring vibration [28]. The bands located at 1305 cm^{-1} is ascribed to the =CH, while the other bands at 1051 $cm^{-1}$and 931 cm^{-1} reflected N−H in-plane deformation vibration and the C−H out of plane vibration [29, 30]. The peaks centered at 884 cm^{-1} is assigned to the hydroxyl group peaks [28]. This proves that flower-like $Mn(VO_3)_2$ precursors is covered with PPy.

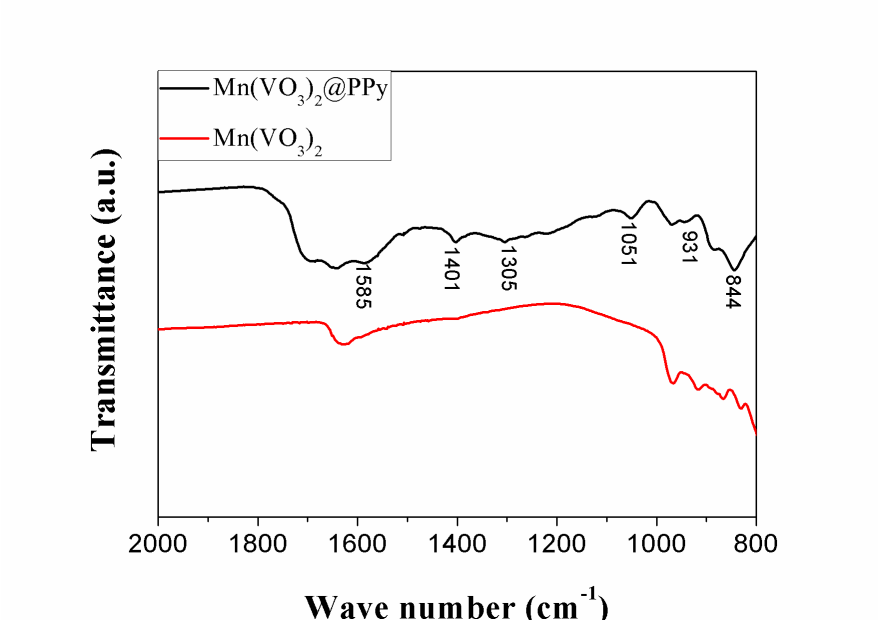

Figure 4. FT-IR spectra of the $Mn(VO_3)_2$ @PPy and $Mn(VO_3)_2$.

3.2. Exploring of the Experimental Conditions

In this work, the effect of time on the morphology of the $Mn(VO_3)_2$ precursor was investigated while other synthesis conditions remain unchanged. It can be seen from Fig. 5a that the morphology are nanoflowers at 6 h. The diameters of the nanoflowers range from 3 to 7 μm without other morphology appearing. Fig. 5b shows a sample formed at 12 h. It can be seen that the morphology of precursor are uniform nanoflowers with the diameter of the spheres become larger. A small amount of nanosheets can be observed on the surface, and a small number of spheres are broken. Fig. 5c is the morphology of the nanoflowers after 18 h. It can be seen that the nanoflowers are destroyed more seriously, while many of the flowers are broken. At the same time, nanoblocks appear in the sample. The FESEM image of the sample after 24 h is shown in Fig. 5d. It is found that there are large numbers of nanoblocks with few nanoflowers, while the length and width of these nanoblocks are all in microscales. However, when the time is too short, there are little products. Obviously, time plays an important role in the preparation of the $Mn(VO_3)_2$ nanoflower precursor. In this method, to obtain the flower-like $Mn(VO_3)_2$ precursor, the optimal time is 12 h.

It has been reported that different anions salts lead to different morphologies of the products [31]. The morphology of manganese oxide is also affected by the anions during the synthesis [32]. Therefore, the effects of different anions on the morphology of $Mn(VO_3)_2$ precursors were investigated. Fig. 5e shows a mixture morphology of nanoblocks and nanoflowers the morphology of the precursor obtained by using $MnSO_4 \cdot H_2O$ appears. Fig. 5f shows the disordered morphology of the precursor obtained by using $MnC_4H_6O_4 \cdot 4H_2O$. Obviously, in the synthesis of the $Mn(VO_3)_2$ flower precursor, different anions have a great influence on the morphology of the final product. In this method, $MnCl_2 \cdot 4H_2O$ was used as the reactant, from it the uniform $Mn(VO_3)_2$ nanoflower precursor could be obtained. To sum up, the optimal conditions to prepare the $Mn(VO_3)_2$ nanoflower precursors

are using $MnCl_2 \cdot 4H_2O$ and NH_4VO_3 as reactants in the mixed solvent (Ethylene glycol: water = 1:1) at 120 °C for 12 h.

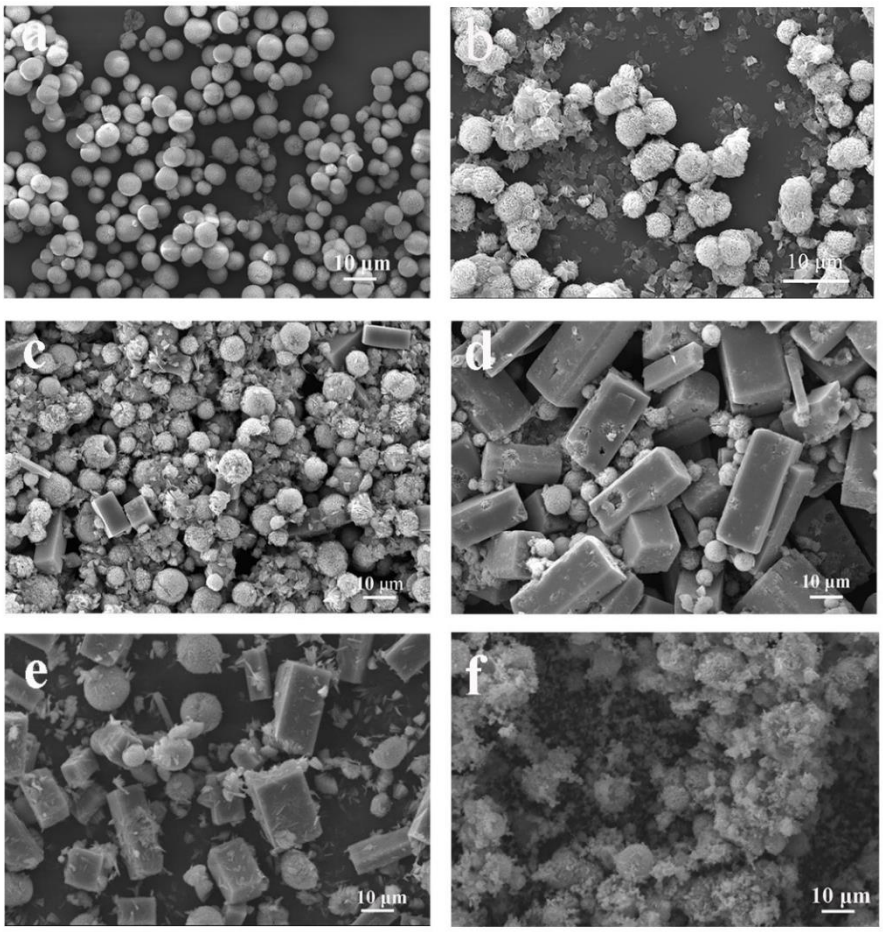

Figure 5. FESEM images of the precursor synthesized by $MnCl_2 \cdot 4H_2O$ at various reaction times: (a) 6h; (b) 12h; (c) 18h; (d) 24h; (e) FESEM image of the precursor prepared by $MnSO_4 \cdot H_2O$; (f) SEM image of the precursor prepared by $MnC_4H_6O_4 \cdot 4H_2O$.

3.3. Electrochemical Performance of $Mn(VO_3)_2$@PPy Nanoflower Composites

The electrochemical performance of $Mn(VO_3)_2$@PPy nanoflower composites for lithium-ion battery has been studied. Fig. 6a shows the cyclic voltammetry (CV) curve of $Mn(VO_3)_2$@PPy nanoflower composites electrode at a scan rate of 0.2 mV s^{-1} within a potential range of 1.5-4.5 V. At the frist cycle, there are two reduction peaks emerging at 2.16 V and 1.73 V, and one broad oxidation peak at 2.80 V. During the second cycle, reduction peak shows two broad peak signals at 2.25 V and 1.94 V, and one broad oxidation peak around 2.93 V. However, during the third cycle, there are only one broden reduction peaks around 2.25 V. This may be due to an irreversible redox reaction [14, 33]. At the second and third cycle, the reduction and oxidation peak positions and currents have less changes than before, which indicates the electrode material becomes more and more stable.

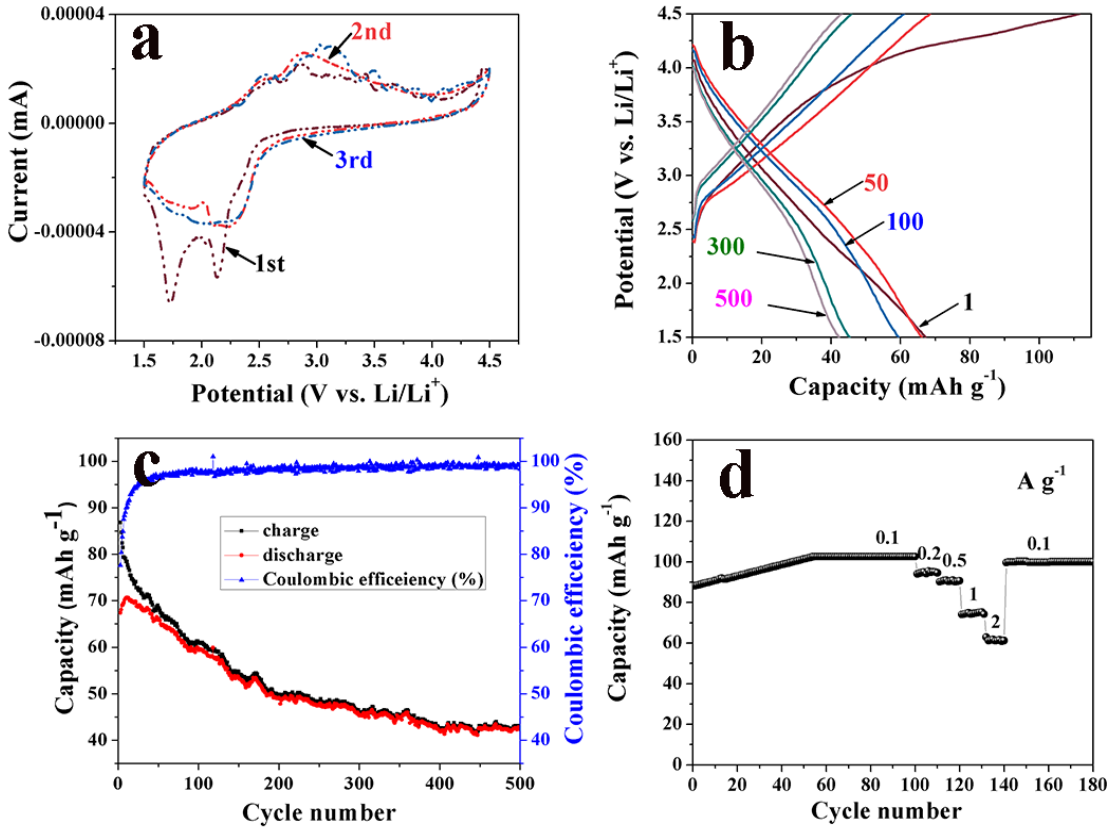

Figure 6. Characterization of the electrochemical properties: (a) CV curves of the $Mn(VO_3)_2$ @PPy nanoflower composites for the first 3 cycles at 0.2 mV s^{-1}; (b) Charge and discharge curves of the electrodes at 1 A g^{-1}; (c) Cycling performance at 1 A g^{-1} for 500 cycles and the Coulombic efficiency; (d) Capacity performances at various cycling rates.

Fig. 6b shows the charge and discharge curves of 1, 50, 100, 300, 500 of the $Mn(VO_3)_2$@PPy nanoflower electrodes when the current density is 1 A g^{-1} in the voltage of 1.5–4.5 V. At a constant current density of 1 A g^{-1}, the first charge capacity is about 110 mAh g^{-1} while the discharge capacity reaches 68 mAh g^{-1}. For the $Mn(VO_3)_2$@PPy nanoflower composites, the specific discharge capacities remain 66.1, 59.4, 45.3 ,42.3 mAh g^{-1} after 50, 100, 300, 500 cycles, respectively. In the test, charge and discharge capacity attenuation are getting smaller and smaller.

Fig. 6c shows the charge-discharge capacity and coulomb efficiency at a current density of 1 A g^{-1} in the voltage interval of 1.5-4.5 V. It can be seen that the $Mn(VO_3)_2$@PPy nanoflower composites have a good cycling performance. At the beginning, the curve increases a little, which is caused by the activation of the lithium battery [19, 33]. Then it decreases gradually and eventually becomes stable, while the coulomb efficiency becomes higher and higher.

Fig. 6d shows the rate performance of $Mn(VO_3)_2$@PPy nanoflower composites at different current densities. When the current density is 0.1 A g^{-1}, the maximum discharge capacity is up to 102.6 mAh g^{-1}, indicating that the as-prepared $Mn(VO_3)_2$@PPy has excellent rate performance. At the same time, the specific discharge capacities of 95.5, 91.0, 75.3 and 62.9 mAh g^{-1} are observed at 0.2, 0.5, 1.0 and 2.0 A g^{-1}, respectively.

Table 1. Comparison of electrochemical properties of the as-prepared $Mn(VO_3)_2$@PPy nanoflowers with some recently reported cathode materials for LIBs

Sample (ref)	Current density (mA g^{-1})	Voltage range (V)	Capacity (mAh g^{-1})
$Mn(VO_3)_2$@PPy nanoflowers	100	1.5-4.5	102.6
$NH_4V_3O_8$ flower[34]	300	1.5-4.0	67
$NH_4V_3O_8$ sheet[34]	300	1.5-4.0	117
KHCF@PPy[35]	100	2.0-4.2	80
$Na_3V_2(PO_4)_3$/Ag+Graphene Composites[36]	118	2.5-4.6	102
rGO/$K_2[(VO)_2(HPO_4)_2(C_2O_4)]$[37]	20	2.3-4.3	100
$LiNi_{0.5}Mn_{1.5}O_4$[38]	118	3.5-5.0	86.2

The electrochemical properties of the as-prepared $Mn(VO_3)_2$@PPy nanoflowers with some recently reportedcathode materials for LIBs are shown in Table 1. Vanadium bronze was usually used as the anode for LIBs in the past. In this work, $Mn(VO_3)_2$@PPy nanoflowers were used as the cathode for LIBs. They exhibited good performs of electrochemical properties compared to some recently reported cathode materials. Besides, the $Mn(VO_3)_2$@PPy nanoflowers provide a new choice of cathode materials for LIBs. They can also form composite with other materials to obtain better electrochemical performance.

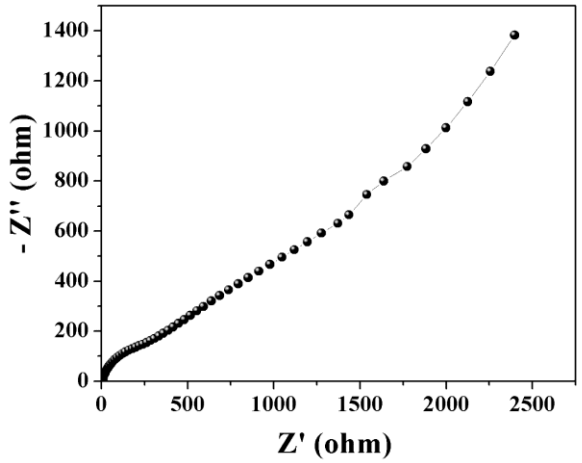

Figure 7. Electrochemical impedance spectra of $Mn(VO_3)_2$ @PPy nanoflower composites.

Fig. 7 shows the electrochemical impedance spectrum of $Mn(VO_3)_2$@PPy nanoflower composites. Obviously, this impedance spectrum is composed of a small arc and a straight line. The small arc of the radius indicates the low resistance of the $Mn(VO_3)_2$@PPy nanoflower composites, which can provide many channels for lithium ions [39]. The flower-like structures increase the contact area between electrode surface and electrolyte, and thus improve the reaction speed of electrode

polarization [17]. Obviously, the lithium transfer rate of the $Mn(VO_3)_2$@PPy flower-like nanostructures is good.

4. CONCLUSIONS

To sum up, flower-like $Mn(VO_3)_2$ precursors with special morphology were successfully prepared by a hydrothermal method and high-temperature calcining without using any template. The PPy was coated on the surface of the flowers by precipitation. The reaction time for hydrothermal preparation of the $Mn(VO_3)_2$ precursor and the effects of anionic reactants were important factors on the morphology of the products. By assembling the $Mn(VO_3)_2$@PPy nanoflower composites as a positive electrode material into a lithium ion battery, the capacity of battery is 102.6 mAh g^{-1} at a current density of 0.1 A g^{-1}. In additions, they have a capacity of 75.3 mAh g^{-1} at a current density of 1 A g^{-1} at a voltage of 1.5-4.5 V, while the capacity approaching 60 mAh g^{-1} after 100 cycles. These experimental results indicate that the $Mn(VO_3)_2$@PPy nanoflower composites could be used as a cathode electrode for lithium-ion batteries.

ACKNOWLEDGMENTS

This work was supported by the Basic Research and Frontier Exploration Project of Beibei (2019-1), the Undergraduate Science and Technology Innovation Project of Southwest University (X201910635062, S201910635029 and P201910635215), and the “Zeng Sumin Cup” Science and Technology Project (School of Materials and Energy, Southwest University, zsm 20190622).

References

1. M.-S. Balogun, W. Qiu, Y. Luo, H. Meng, W. Mai, A. Onasanya, T.K. Olaniyi, Y. Tong, *Nano Research*, 9 (2016) 2823-2851.
2. S. Zhu, J. Li, X. Deng, C. He, E. Liu, F. He, C. Shi, N. Zhao, *Advanced Functional Materials*, 27 (2017) 1605017.
3. Y. Lu, J. Nai, X.W.D. Lou, *Angewandte Chemie International Edition*, 57 (2018) 2899-2903.
4. G. Zubi, R. Dufo-López, M. Carvalho, G. Pasaoglu, *Renewable and Sustainable Energy Reviews*, 89 (2018) 292-308.
5. M. Winter, B. Barnett, K. Xu, *Chemical reviews*, 118 (2018) 11433-11456.
6. B. Diouf, R. Pode, *Renewable Energy*, 76 (2015) 375-380.
7. Y.L. Kai Liu, Dingchang Lin, Allen Pei, Yi Cui, *Science Advances*, 4 (2018) 9820.
8. G.X. Wang, L. Yang, Y. Chen, J.Z. Wang, S. Bewlay, H.K. Liu, *Electrochimica Acta*, 50 (2005) 4649-4654.
9. Y. Fu, A. Manthiram, *The Journal of Physical Chemistry C*, 116 (2012) 8910-8915.
10. X.-W. Gao, Y.-F. Deng, D. Wexler, G.-H. Chen, S.-L. Chou, H.-K. Liu, Z.-C. Shi, J.-Z. Wang, *Journal of Materials Chemistry A*, 3 (2015) 404-411.
11. X. Sun, H. Zhang, L. Zhou, X. Huang, C. Yu, *Small*, 12 (2016) 3732-3737.
12. Y. Song, H. Wang, W. Yu, J. Wang, G. Liu, D. Li, T. Wang, Y. Yang, X. Dong, Q. Ma, *Journal of Power Sources*, 405 (2018) 51-60.
13. H. Kang, Y. Liu, M. Shang, T. Lu, Y. Wang, L. Jiao, *Nanoscale*, 7 (2015) 9261-9267.

14. S. Zhang, H. Yun, H. Yu, *Journal of Alloys and Compounds*, 735 (2018) 700-706.
15. B. Zhang, X.-w. Wang, J.-f. Zhang, *RSC Advances*, 4 (2014) 49123-49127.
16. J.-f. Zhang, X.-w. Wang, B. Zhang, C.-l. Peng, H. Tong, Z.-h. Yang, *Electrochimica Acta*, 169 (2015) 462-469.
17. Y. Liu, M. Xu, B. Shen, Z. Xia, Y. Li, Y. Wu, Q. Li, *Journal of Materials Science*, 53 (2017) 2045-2053.
18. W. Huang, S. Gao, X. Ding, L. Jiang, M. Wei, *Journal of Alloys and Compounds*, 495 (2010) 185-188.
19. Z. Lei, J. Yang, Y. He, Y. Shao, S.X. Mao, C. Wang, Y. Nuli, J. Wang, *Journal of Alloys and Compounds*, 695 (2017) 1813-1820.
20. L.Z. Pei, Y.Q. Pei, Y.K. Xie, C.G. Fan, H.Y. Yu, *CrystEngComm*, 15 (2013) 1729.
21. B. Sambandam, V. Soundharrajan, J. Song, S. Kim, J. Jo, P.T. Duong, S. Kim, V. Mathew, J. Kim, *Journal of Power Sources*, 350 (2017) 80-86.
22. H.I. Sung-SooKim, Masataka Wakihara, *Solid State Ionics*, 139 (2001) 57-65.
23. L.Z. Pei, N. Lin, T. Wei, H.Y. Yu, *Journal of Experimental Nanoscience*, 11 (2015) 197-214.
24. H. Peng, J. Ding, N. Wang, G. Li, *Materials Letters*, 63 (2009) 1404-1406.
25. S. Zhang, R. Hu, L. Liu, D. Wang, *Materials Letters*, 124 (2014) 57-60.
26. X. Yang, Y. Tian, S. Sarwar, M. Zhang, H. Zhang, J. Luo, X. Zhang, *Electrochimica Acta*, 311 (2019) 230-243.
27. D. Zhang, Y. Chen, X. Yu, H. Huang, L. Li, L. Wei, *Materials Research Express*, 6 (2019) 085044.
28. J. Li, L. Cui, X. Zhang, *Applied Surface Science*, 256 (2010) 4339-4343.
29. X.-B. Zhong, H.-Y. Wang, Z.-Z. Yang, B. Jin, Q.-C. Jiang, *Journal of Power Sources*, 296 (2015) 298-304.
30. X. Gu, Y. Yang, Y. Hu, M. Hu, J. Huang, C. Wang, *Journal of Materials Chemistry A*, 3 (2015) 5866-5874.
31. C. Tang, W. Sun, J. Lu, W. Yan, *Journal of colloid and interface science*, 416 (2014) 86-94.
32. L. Zhou, J. Zhang, J. He, Y. Hu, H. Tian, *Materials Research Bulletin*, 46 (2011) 1714-1722.
33. D. Deng, Y. Zhang, G. Li, X. Wang, L.H. Gan, L. Jiang, C.R. Wang, *Chemistry, an Asian journal*, 9 (2014) 1265-1269.
34. Y. Cheng, J. Huang, J. Li, L. Cao, Z. Xu, J. Wu, S. Cao, H. Hu, *Electrochimica Acta*, 212 (2016) 217-224.
35. Q. Xue, L. Li, Y. Huang, R. Huang, F. Wu, R. Chen, *ACS applied materials & interfaces*, 11 (2019) 22339-22345.
36. M.S. Choi, H.S. Kim, Y.M. Lee, S.M. Lee, B.S. Jin, *Journal of nanoscience and nanotechnology*, 15 (2015) 8937-8942.
37. I.N. Sivagami, K. Prasanna, P. Santhoshkumar, Y.N. Jo, S.H. Kang, T.H. Kim, C.W. Lee, *Journal of nanoscience and nanotechnology*, 17 (2017) 8061-8066.
38. J.-J. Pan, B. Chen, Y. Xie, N. Ren, T.-F. Yi, *Materials Letters*, 253 (2019) 136-139.
39. Y. Liu, B.H. Zhang, S.Y. Xiao, L.L. Liu, Z.B. Wen, Y.P. Wu, *Electrochimica Acta*, 116 (2014) 512-517.